Observations of Fluxes and Inland Breezes over a Heterogeneous Surface

L. MAHRT, JIELUN SUN, AND DEAN VICKERS

Oceanic and Atmospheric Sciences, Oregon State University, Corvallis, Oregon

J. I. MACPHERSON

Flight Research Laboratory, National Research Council, Ottawa, Canada

J. R. PEDERSON

California Air Resources Board, Sacramento, California

R. L. DESJARDINS

Centre for Land and Biological Resources Research, Agriculture Canada, Ottawa, Canada

(Manuscript received 30 August 1993, in final form 20 December 1993)

ABSTRACT

Repeated aircraft runs at about 33 m over heterogeneous terrain are analyzed to study the spatial variability of the mesoscale flow and turbulent fluxes. An irrigated area, about 12 km across, generates a relatively cool moist inland breeze. As this air flows out over the warmer, drier surrounding land surface, an internal boundary layer develops within the inland breeze, which then terminates at a well-defined inland breeze front located about 1 1/2 km downstream from the change of surface conditions. This front is defined by horizontal convergence, rising motion, and sharp spatial change of moisture, carbon dioxide, and ozone.

Both a scale analysis and the observations suggest that the overall vertical motion associated with the inland breeze is weak. However, the observations indicate that this vertical motion and attendant vertical transport are important in the immediate vicinity of the front, and the inland breeze does lead to significant modification of the turbulent flux. In the inland breeze downstream from the surface wetness discontinuity, strong horizontal advection of moisture is associated with a rapid increase of the turbulent moisture flux with height. This large moisture flux appears to be partly due to mixing between the thin moist inland breeze and overlying drier air.

As a consequence of the strong vertical divergence of the flux in the transition regions, the fluxes measured even as low as a few tens of meters are not representative of the surface fluxes. The spatial variability of the fluxes is also interpreted within the footprint format. Attempts are made to reconcile predictions by footprint and internal boundary-layer approaches.

1. Introduction

Boundary-layer flow over surface heterogeneity is generally posed in terms of either *internal boundary layers, blending height,* or *footprint signatures.* In pure form, these three conceptual approaches make quite different assumptions on the response of the turbulence and time-averaged flow to the surface variations. In addition, surface heterogeneity of sufficiently large scale may generate flow of cool air from cool wet surfaces to warm dry surfaces, sometimes referred to as *inland breezes.* A plausible geometry of these different phenomena is sketched in Fig. 1 partly based on data analysis of flow over heterogeneous surfaces carried out in this study. One of the goals of this paper is to compare the internal boundary-layer approach and the footprint approach in terms of aircraft turbulence data collected over a heterogeneous surface. These particular observations are well below any blending height. A second goal is to document circulations driven by the surface heterogeneity (*inland breezes*), which lead to a special type of internal boundary layer. Such local circulations have previously been studied primarily from a modeling point of view (Segal and Arritt 1992); the present study contributes observational evidence.

Definition of the internal boundary layer assumes that the change of surface conditions can be described by a near discontinuity and that the air influenced by surface conditions downstream from the discontinuity is limited to a definable layer adjacent to the surface; that is, the top of the internal boundary layer is the maximum vertical extent of the disturbance generated

Corresponding author address: Dr. Larry Mahrt, Oceanic and Atmospheric Sciences, Oregon State University, Corvallis, OR 97331.

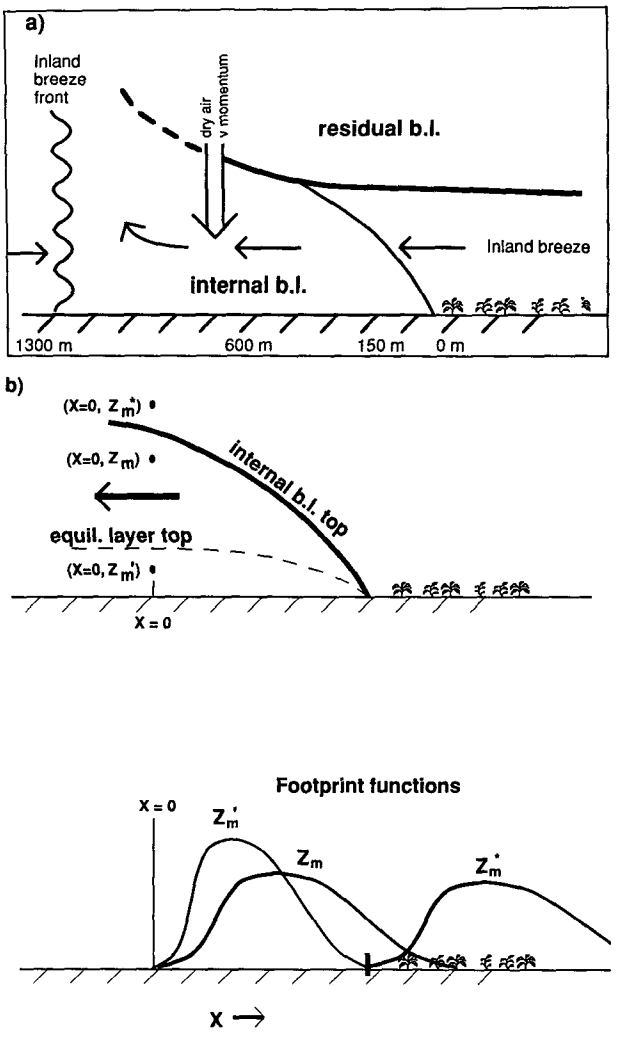

FIG. 1. (a) Plausible sketch of the internal boundary layer developing within the inland breeze as it flows from the wet area out over a dry heated surface. The inland breeze terminates in a front downstream from the change of surface conditions. The horizontal spacing of the features in the inland breeze is based on the data analysis in sections 3–4. (b) Plausible footprint function for fluxes measured above the internal boundary layer (z_m^*), within the internal boundary layer but above the equilibrium layer (z_m) and within the equilibrium layer (z_m'). Here x is directed in the upstream direction as in footprint convention. See Eq. (1) for definitions.

by a change of surface conditions (Brutsaert 1982). The lowest part of the internal boundary layer is in equilibrium with the new surface (Garratt 1990) and referred to as the *equilibrium layer* (Fig. 1b). In transition regions downstream from changes of surface conditions, the flux may be quite different from that predicted from local similarity theory. For example, in flow of cool air from the irrigated region to an unirrigated region, the heat flux may initially reach twice the equilibrium value before reaching equilibrium with the heated dry surface farther downstream (Garratt 1992).

The usual formulations for mesoscale growth of the internal boundary layer over a heated surface due to entrainment across the capping inversion do not apply to microscale growth of the internal boundary layer, which is not capped by an observable inversion. The primary example of the mesoscale internal boundary layer is the growth of a heated layer within the sea breeze downstream from the coast. In this study, the microscale internal boundary layer refers to smaller-scale surface heterogeneity where the internal boundary layer does not grow to the top of the planetary boundary layer. The top of the microscale internal boundary layer represents the limit of the most vigorous thermals generated by the warm surface and tilted by the airflow. Although the definition of *entrainment* in the literature has been vague and flexible, it may not be practical to force this concept on the growth of the microscale internal boundary layer. For example, over the cool wet surface, the flow above the internal boundary layer (*residual layer,* Fig. 1) contains turbulence generated from surface heating farther upstream. Although this layer has not been explicitly studied, Garratt and Ryan (1989) and Raynor et al. (1979) observed residual turbulence above growing internal boundary layers.

If the surface heterogeneity is not organized into well-defined regions of constant surface conditions, the concept of an internal boundary layer becomes ambiguous. In such cases, internal boundary layers may grow inside of other internal boundary layers such that the various internal boundary layers and large boundary-layer eddies cannot be separated. If the surface heterogeneity occurs on a sufficiently small scale and is sufficiently random, the concept of a blending height might be applicable (Mason 1988; Claussen 1990; Wood and Mason 1991). Above the blending height, the fluxes are in statistical equilibrium with the spatially averaged surface conditions and becomes independent of spatial position. A similar concept is expressed in Raupach (1993), where the atmospheric boundary layer responds to a spatial average of the surface features if they occur on sufficiently small scales (microscale heterogeneity).

The footprint signature of the flux at a given height above ground can be estimated in terms of a weighted average of spatially varying surface conditions (Fig. 1b). For example, the observed flux $F(0, z_m)$, at position $x = 0$ and observational level z_m, can be expressed as (Schuepp et al. 1990; Horst and Weil 1992; Leclerc and Thurtell 1990)

$$F(0, z_m) = \int_0^\infty Q(x)\mathrm{FP}(x, z_m)dx, \qquad (1)$$

where $Q(x)$ is the surface distribution of the flux or some other quantity; $\mathrm{FP}(x, z_m)$ is a weighting function (footprint function), which relates the observed flux at position $x = 0$ to the upstream surface flux distribution;

and x is increasing positive in the upstream direction. The footprint function $\mathrm{FP}(x, z_m)$ is normally specified as a smooth function that reaches a maximum upstream from $x = 0$ and then gradually decreases farther upstream (Gash 1986; Schuepp et al. 1992).

If at a certain height the area of weighting of surface conditions becomes large compared to the scale of the surface heterogeneity, then the flux becomes independent of spatial position and the concept of a blending height becomes applicable. Then the footprint approach becomes undefined since the flux $F(0, z_m)$ no longer depends explicitly on the spatial distribution of the surface flux $Q(x)$.

The footprint approach is traditionally based on diffusion arguments, and the footprint-adjusted fluxes vary smoothly in space. In contrast, the internal boundary layer may be generated by a discontinuity of surface temperature and is sometimes visualized in terms of a well-defined vertical jump in properties at the top of the internal boundary layer. Nonetheless, it is possible to qualitatively discuss the footprint function for flow over a surface discontinuity. Figure 1b sketches a plausible relationship between the footprint function and the concept of an internal boundary layer generated by a surface heat flux discontinuity. For points above the internal boundary layer (z_m^*), the flow depends only on surface conditions upstream from the surface discontinuity. Therefore, the footprint function for this flow is zero between $x = 0$ and the surface discontinuity and becomes nonzero only upstream from the surface discontinuity. Flow within the internal boundary layer but above the equilibrium layer (Fig. 1b, z_m) is influenced by the surfaces both upstream and downstream from the surface discontinuity, and the footprint function should be nonzero on both sides of this surface discontinuity. Flow within the equilibrium layer (z_m') is influenced only by the surface downstream from the discontinuity and its footprint function is nonzero only between $x = 0$ and the upstream discontinuity. The possible connection between the internal boundary-layer and footprint approaches will be explored in the data analysis of section 5.

In addition to modulation of turbulence fluxes, the surface heterogeneity may also induce its own circulation. With sufficiently weak ambient flow, lower hydrostatic pressure tends to form over the warmer surfaces and relatively higher hydrostatic pressure over adjacent cooler surfaces. The resulting inland breeze flows from cooler to warmer surfaces and an internal boundary layer develops within the inland breeze as it flows over the heated surface (Fig. 1a). Several studies indicate that the scale of the surface heterogeneity must exceed a certain critical horizontal scale before generating such mesoscale circulations (Segal et al. 1989; Yan and Anthes 1988; Segal and Arritt 1992; Hechtel et al. 1990). This required critical scale increases with ambient flow speed. Segal et al. (1989), Segal and Arritt (1992), and Hadfield et al. (1992) show how even weak ambient flow may eliminate circulations driven by surface heterogeneity, particularly heterogeneity on smaller scales. In addition to masking effects of the synoptic-scale flow, the generation of inland breezes must compete with transient mesoscale motions. The energy of such mesoscale motions is often significant (Lilly 1983), perhaps due to generation by various instabilities (Emanuel 1983) including inertial gravity waves and convection waves (Clarke et al. 1986). Transient mesoscale motions occurred in the present datasets (Mahrt et al. 1993) but did not seriously mask the signature of the inland breezes.

In previous observational studies, inland breezes have been isolated mainly in the case of contrasts between agricultural and forest regions (*forest breezes*) as in André et al. (1989), Pinty et al. (1989), Noilhan et al. (1991), and Mahrt and Ek (1993). Forest breezes were predicted by the numerical simulations of André et al. (1989), Pinty et al. (1989), Bougeault et al. (1991), and Bechtold et al. (1991). On a smaller scale, Doran et al. (1992) observed a farm breeze responding to irrigation within a dry steppe region.

As the inland breeze flows over warmer surfaces, the resulting internal boundary layer presumably grows to the top of the inland breeze (Fig. 1). Apparently this process is sufficiently rapid, and any inversion at the top of the inland breeze is sufficiently weak that the inland breeze may not be identifiable after propagating a short distance over the heated ground (Mahrt and Ek 1993). The present development examines the horizontal structure of inland breezes generated by an irrigated area, 10–15 km across, and surrounded by drier, warmer surfaces. The inland breeze in this study is better defined and better sampled compared to Mahrt and Ek (1993) and other previous observational studies.

2. The data

This work analyzes data from the California Ozone Deposition Experiment (CODE) consisting of eight 33-km legs flown at about 33 m above flat terrain on 30 July 1991 (flight 19) between approximately 1045 and 1245 local solar time. On this day, the large-scale winds were weak, about 2 m s^{-1} from NNW. Data were also collected over this same flight track on 23 July 1991 (flight 13) when the ambient flow (Fig. 2) averaged about 4 m s^{-1} from NNW. On this day, the observations were carried out between 1300 and 1500 local solar time. Both days are characterized by clear skies.

The instrumentation is described in MacPherson (1992) and MacPherson et al. (1993); the flow situation for these two days is described in Mahrt et al. (1993). The data analyzed here were sampled at 16 Hz and anti-alias filtered at 5.5 Hz corresponding to a spatial resolution of about 10 m (average airspeed 58 m s^{-1}).

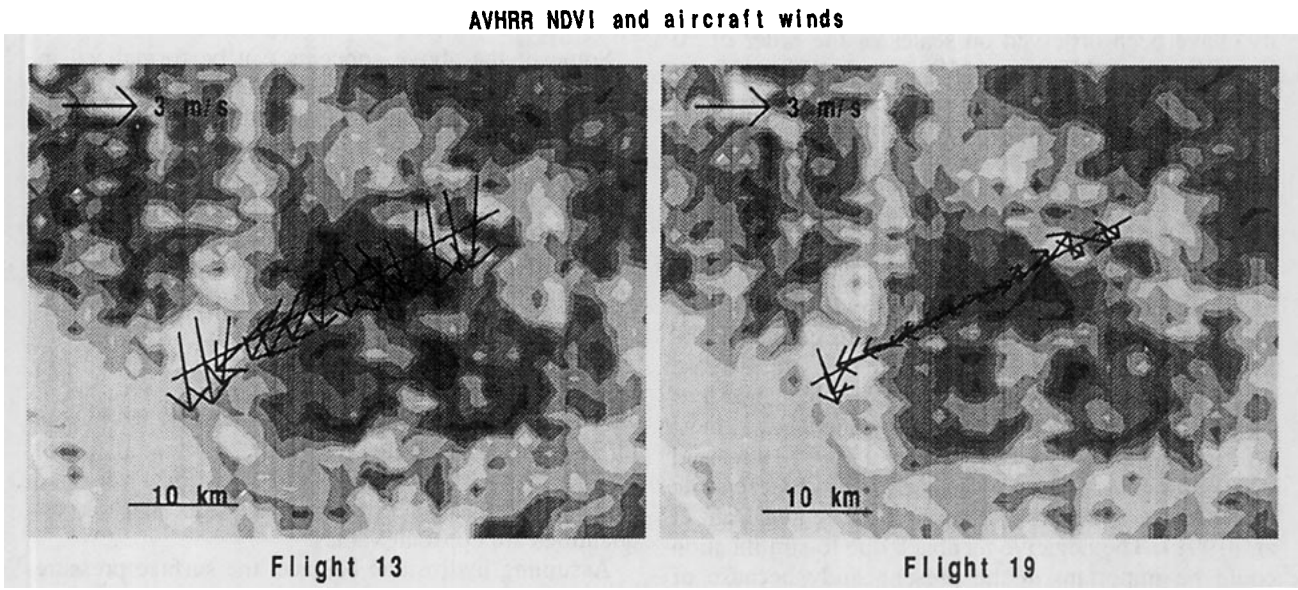

FIG. 2. AVHRR NDVI data for flights 13 and 19 and wind vectors based on averages of components over 2-km segments and composited over the eight runs. Shading represents different numerical classes of NDVI, white represents the interval (−0.1, 0), and the darkest shading represents the interval (0.5–0.6).

The aircraft track for the present data overlays irrigated croplands, mainly cotton, and nonirrigated areas, mainly bare soil and cut hay. These variations are shown in Fig. 3 in terms of the normalized difference of vegetation index (NDVI). This index is computed from aircraft-measured reflectance at two wavelengths, one centered at 0.73 μm and one centered at 0.66 μm. The NDVI is used as a measure of surface vegetation (e.g., Tucker 1979). The surface heterogeneity in the present field program is well defined by the NDVI (Fig. 3), which is highly correlated with the surface radiation temperature ($r > 0.9$). The two-dimensional map of NDVI constructed from NOAA Advanced Very High Resolution Radiometer (AVHRR) satellite data (Fig. 2) agrees reasonably well with the pattern along the aircraft track after taking into account the lower spatial resolution of 1 km for the AVHRR data.

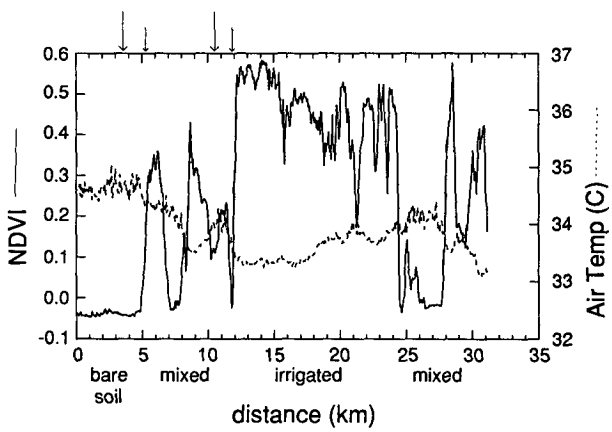

FIG. 3. Composited spatial variation of NDVI (solid) and air temperature (dashed) composited for the eight flight legs for flight 19. Large arrows above figure indicate location of center of expanded composites about the breeze fronts (Fig. 5), while small arrows indicate center of expanded composites about the NDVI boundaries (Fig. 6).

The flight track can be divided into an intensely irrigated region in the center, about 12 km across, areas of mixed land use about 7 km across on each side of the irrigated region, and relatively dry areas at each end of the flight region with little active vegetation (Fig. 3). The surface radiation temperature varies by about 20°C between the irrigated croplands and nonirrigated areas. The air temperature at 33 m in this study varies by 2°–3°C between irrigated and nonirrigated areas (Fig. 3), which is comparable to the variations in Tsukamoto et al. (1992) and a bit larger than those reported in Doran et al. (1992).

3. Direct mesoscale transport

a. Potential mechanisms

Several distinct influences on generation of mesoscale circulations from surface heterogeneity can be identified from previous studies.

(i) Horizontal diffusion seemed to prevent mesoscale circulations from developing over small-scale heterogeneity (on the order of 10 km) in the numerical modeling work of Anthes (1984) and Dalu and Pielke (1993). Horizontal diffusion on this scale has not been

measured. Lake and river breezes (strong heterogeneity) have been observed on scales of the order of 10 km (Oliveira and Fitzjarrald 1993) and smaller (Yoshino 1975; Bitan 1981).

(ii) Pressure adjustments resulting from mesoscale vertical motion in the presence of stable stratification above (or within) the boundary layer act as a negative feedback, which preferentially inhibits the development of circulations driven by smaller-scale surface heterogeneity (Smith and Mahrt 1981). More specifically, rising motion driven by mesoscale low pressure over the heated surface leads to adiabatic cooling in the overlying stratified flow. This cooling acts to increase the hydrostatic pressure at lower levels and thus weaken the circulation. This negative feedback is most effective at smaller scales (Smith and Mahrt 1981) and appears to contribute to the preferred sea-breeze scale found in the analysis of Rotunno (1983) and Dalu et al. (1991). The negative feedback due to stratification could be important in the present study because of strong stratification in the inversion layer above the boundary layer. The study of Smith and Mahrt (1981) indicates that the strength of the circulation due to differential heating varies inverse linearly with the Brunt–Väisälä frequency. As an additional influence, nonhydrostatic pressure adjustments on scales of the order of 1 km might be quite large (Pielke 1984; Hsu 1987).

(iii) Small-scale surface heterogeneity with nonzero mean wind may fail to generate significant circulations because the *depth of the modified flow* does not have sufficient time to grow to a significant depth before the flow encounters a new surface. This aspect can be posed in terms of growth of the *internal boundary layer* [Garratt (1992); see Eq. (10) in section 4 of this study], or in the case of flow over a warmer surface, *tilting* of the thermally modified column (Anthes 1984) and displacement of the convergence pattern (Manqian and Jinjun 1993). The magnitude of the hydrostatic pressure perturbation is proportional to the depth of the modified air and therefore small when the internal boundary layer of modified air does not deepen sufficiently before the airflow encounters a new surface. In the basic governing equations, the internal boundary-layer development, or tilting effect, can be identified with the horizontal advection of temperature in the presence of a change of surface heat flux. The horizontal advection of momentum also acts to compete with the circulation driven by the surface heterogeneity. These advective effects are most important when the scale of the heterogeneity is small. In the study of Hadfield et al. (1992), even weak mean winds greatly reduced the influence of differential surface heating. The main exception appears to be flow from a warm surface to a cold surface where advective effects may enhance the circulation driven by differential heating (Avissar and Chen 1993).

b. Scale analysis

Some of the above concepts can be formalized in terms of a simple scale analysis. The goal of the scale analysis is to estimate the order of magnitude of the vertical motion generated by the perturbation hydrostatic pressure field associated with differential surface heating. This analysis begins by assuming that horizontal advection due to the heterogeneity is the same order of magnitude as the perturbation pressure gradient induced by the heterogeneity. Then the scaled version of the equation of motion can be written as

$$UU^*/L = \alpha_0 P^*/L, \tag{2}$$

where U is the total mean flow, U^* is the scale value for the perturbation flow, L is the horizontal length scale of the surface feature, and α_0 is the basic-state specific volume. As in traditional scale analysis, all quantities are constant values.

Assuming hydrostatic balance, the surface pressure perturbation can be written as

$$P^* = (T^*/T_0)\rho_0 gH, \tag{3}$$

where H is a scale value for the depth of the layer influenced by the surface change, T^* is the scale value of the perturbation temperature (neglecting the influence of moisture on buoyancy), and T_0 is the basic-state temperature. Combining (2) and (3),

$$U^* = \frac{1}{U}(T^*/T_0)gH. \tag{4}$$

The temperature perturbation is estimated by assuming that the temperature change due to the divergence of the turbulent heat flux is the same order of magnitude as the temperature advection. For example, in flow over a heated surface, the local temperature change due to the turbulent heat flux divergence is counteracted by cold air advection. Then

$$UT^*/L = [w'T']/H.$$

Solving for T^* and substituting the above equation into (4),

$$U^* = (1/U^2)([w'T']/T_0)gL. \tag{5}$$

In the case of no synoptic-scale flow, $U = U^*$ and the perturbation velocity becomes

$$U^* = ([w'T'](g/T_0)L)^{1/3}, \tag{6}$$

where U^* will be called the *mesoconvective velocity scale* in recognition of its analogy to the free-convection velocity scale w^*. In fact, $U^* = w^*(L/h)^{1/3}$, where h is the depth of the boundary-layer flow.

The vertical motion scale W^* is estimated from the continuity equation as

$$W^* = U^*H/L. \tag{7}$$

For the case of weak mean wind, W^* can be estimated by substituting (6) into (7), in which case

$$W^* = (H/L)([w'T'](g/T_0)L)^{1/3}. \quad (8)$$

Combining (5) and (7) for the case of significant mean wind yields

$$W^* = (1/U^2)([w'T']/T_0)gH. \quad (9)$$

The perturbation vertical velocity is inverse quadratically related to the mean flow because the mean flow reduces the perturbation momentum both directly through momentum advection and indirectly through temperature advection (reduction of the hydrostatic pressure perturbation). In other terms, the greater the mean speed, the less time an air parcel spends over the surface feature, and the less the modification of the flow. Note that W^* in (9) does not explicitly depend on the length scale; however, the depth of the modified flow H is some function of L.

c. Application to CODE data

The aircraft winds (Fig. 2) suggest that mesoscale divergence over the irrigated area is induced by surface heating, which surrounds the irrigated area. The horizontal scale is chosen to be $L = 20$ km to represent roughly the distance from the center of the irrigated area to the center of the unirrigated area. The following estimate chooses $T_0 = 300$ K and $[w'T'] = 0.1$ K m s^{-1} based on the heat flux value in the nonirrigated region. Then U^* estimated from (6) is approximately 4 m s^{-1}. The actual amplitude of the horizontal flow is about 2 m s^{-1} (Fig. 2). The actual magnitude of the mesoscale flow might be less than estimated from (6) because of the difficulty of defining scaling variables and the neglect of surface drag and adiabatic pressure adjustments discussed above.

Because the aircraft level of 33 m is relatively close to the surface, the observed vertical motion might be significantly larger at higher levels within the mesoscale motion. For comparison with the data, (8) is applied with $z = 33$ m instead of the depth of the circulation. For a horizontal length scale of 20 km, the vertical velocity scale at 33 m is estimated from (8) to be only about 3 cm s^{-1}, too small to reliably measure. The difference between observed vertical motions averaged over the irrigated area and averaged over the drier area is too small to distinguish from sampling errors. Observed significant vertical motion, however, is concentrated in narrow zones, referred to as *inland breeze fronts* and sketched in Fig. 4. For example, the diverging outflow from the irrigated area terminates in frontal zones, here observed both east and west of the irrigated area. The most persistent fronts occur west of the irrigated area where the contrast between the green vegetated areas and dry areas is better defined. Easterly outflow (inland breeze) from the irrigated area leads to convergent frontal zone as sketched in Fig. 4. This inland breeze front is located 1–2 km downstream (west) from the edge of the irrigated area over the area of mixed surface conditions. A second inland breeze front (Fig. 4) develops at the leading edge of air flowing from the mixed surface region out over heated dry ground. This second front is located 1–2 km downwind (west) of the edge of the area of mixed surface conditions.

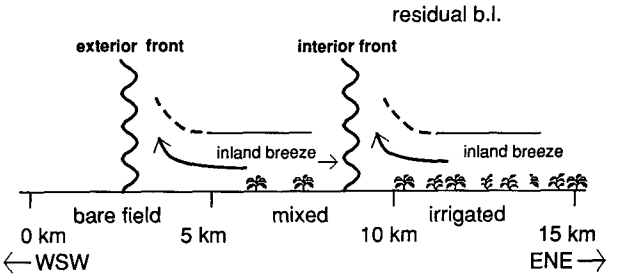

FIG. 4. Schematic of inland breeze fronts.

The above scale analysis provides an estimation of the averaged circulation on the scale of the heterogeneity but does not recognize the concentration of the vertical motion into narrow frontal zones. The inland breeze fronts are not obvious features of numerical simulations (e.g., Segal et al. 1988); resolution of such fronts presumably requires very small grid size. Such fronts are now analyzed in more detail.

d. Inland breeze front

The two inland breeze fronts west of the irrigated area will be referred to as the exterior and interior breeze fronts (Fig. 4). Since the position of the front sometimes changes, simple compositing of the different time series leads to artificial smoothing of the frontal zone. For example, the exterior inland breeze extends about 2 km into the dry region during the early part of the observational period. This penetration recedes to about 1 km later in the observational period. The front may recede due to the increase of buoyancy-driven mixing over the heated ground later in the observational period. The interior inland breeze front is more stationary, located about 1.3 km west of the irrigated area. The initial evolution of the inland breeze and the behavior of the inland breeze later in the afternoon cannot be studied here because the aircraft could sample for only a 2-hour period, here 1045–1245 solar time. Based on the simulations of Avissar and Chen (1993), the inland breeze circulation is expected to continue and perhaps strengthen during the afternoon.

To study the structure of the flow near the front, samples 4 km wide are selected, centered about the front, for each of the eight aircraft runs. The position selection was based primarily on convergence of the velocity component along the flight track. These samples are composited over the eight aircraft runs (Fig.

5) to reduce the influence of turbulent fluctuations and sampling errors although both influences are not completely eliminated. The NDVI discontinuities east of the fronts are somewhat smoothed since the absolute position of the center of the samples varies. The average position of these fronts are indicated with large arrows in Fig. 3.

For future use, 4-km samples are also collected centered at the NDVI discontinuity at the western edge of the irrigated area (interior NDVI boundary) and centered about the discontinuity between the large bare field at the western end of the run and the area of mixed vegetation (exterior NDVI boundary). For each discontinuity, these samples are composited over the eight runs and shown in Fig. 6. The fluxes from these 4-km samples are also composited (Fig. 6). The fluxes were first computed for each run using a 375-m moving average. This narrow window better resolves the rapid spatial variations of the flux but excludes the flux due to larger-scale eddies.

The inland breeze front (Fig. 5) separates the cool, moist air with small carbon dioxide and ozone content from heated drier air with larger carbon dioxide and ozone content. The stronger northerly flow over the warmer surface west of the breeze front appears to be partly related to enhanced downward mixing of NNW flow. The regional boundary layer is characterized by flow of a few meters per second from the N or NW as inferred from an aircraft sounding at the end of the track and balloon soundings 125 km north-northwest of the aircraft track. The observed flow over the heated ground west of the exterior breeze front is therefore probably part of the convectively mixed boundary layer. The downward mixing of ambient momentum west of this front appears to contribute to the maintenance of horizontal convergence at the front.

The horizontal convergence in the exterior breeze front produces rising motion averaging about 60 cm s^{-1} over a width of 200 m. The interior breeze front induces rising motion averaging about 30 cm s^{-1} over a width of about 600 m. Spread out over 20 km, this convergence would lead to average rising motion 1.5 cm s^{-1}, which is the same order of magnitude but less than the 3 cm s^{-1} predicted by the scale analysis of section 3b. The rising motion for both fronts seems to induce some adjacent weak sinking motion.

The width of the frontal updraft is a few hundred meters and is comparable to the size of the transporting turbulent eddies. This updraft, however, is apparently forced by the mesoscale inland breeze and therefore is part of the mesoscale circulation. A second updraft, nearly as strong as at the breeze front, occurs in the composited structure 600 m west of the exterior breeze front, and a significant updraft also occurs 900 m east of the front (Fig. 5). This composited spatial structure suggests a preferred spacing of eddies organized by the front. With this notion, the eddies farther from the front would be less defined due to some variations in the spacing (jittering) and resulting smoothing from the compositing.

While most of the mesoscale spatial change of moisture, carbon dioxide, and ozone are concentrated in the frontal zone (Fig. 5), much of the mesoscale spatial variation of the temperature occurs within the inland breeze. The temperature in the inland breeze behind the front warms significantly in the downstream direction (Figs. 5–6) due to significant surface heat flux and suspected downward heat flux at the top of the inland breeze.

e. Mesoscale transport

The concentrated vertical motion at the exterior breeze front leads to significant upward flux of heat. Outside this zone, however, the vertical motion and heat flux due to the inland breeze circulation are small. The mesoscale flux for the entire record was estimated from the deviations from the record averages. This mesoscale flux was about 10% greater for moisture and 30% greater for heat compared to the turbulent fluxes based on deviations from the 1-km mean. Presumably, this mesoscale flux increases with height. This mesoscale flux would be required for comparison with surface fluxes or construction of a surface energy budget.

f. Significant ambient flow

The influence of more significant ambient flow is now examined using the data from flight 13 when winds upstream from the irrigated area average about 4 m s^{-1} from NNW. This ambient flow eliminates the inland breeze; however, the cooler air over the irrigated area does induce diffluence of the ambient flow (Fig. 2). Consequently, the influence of differential heating due to the spatial pattern of irrigation exerts an important influence on the ambient flow even when the ambient flow is not weak. The flow component in the direction of the flight path diverges outward from the irrigated area and terminates in well-defined fronts both east and west of the irrigated area. These fronts occur closer to the irrigation boundaries compared to the fronts on flight 19. The fronts for flight 13 are well defined in terms of the stronger northerly flow component on the hot dry side of the front, suggesting the important role of downward momentum flux over the heated ground.

4. Internal boundary layer

a. Growth

The previous section indicated that the outflow of cool moist air from the irrigated area extends 1–2 km over the heated ground. Within this inland breeze, an internal boundary layer develops in response to the surface heating. The role of the roughness change is thought to be secondary although the roughness lengths

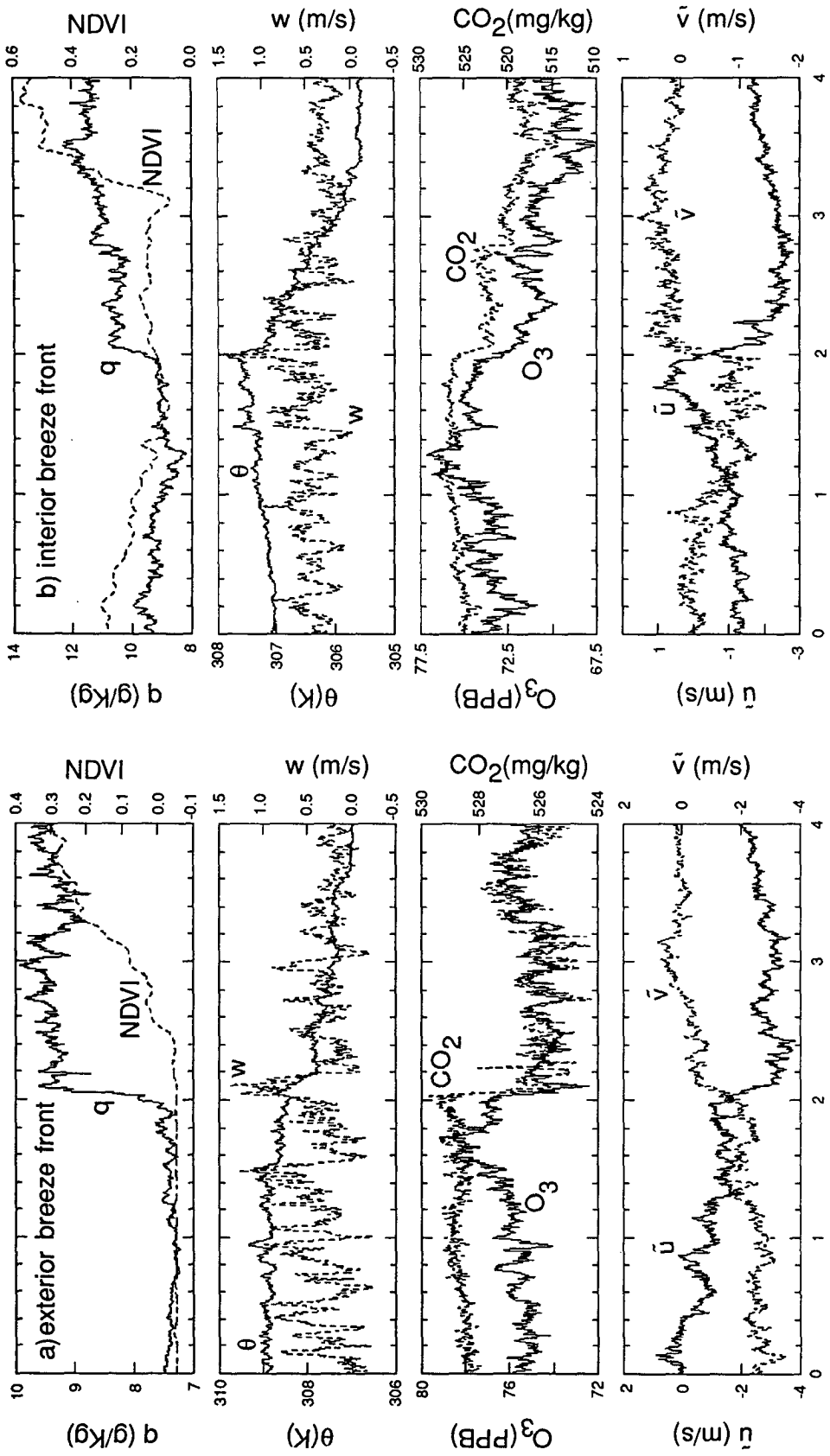

FIG. 5. Composited structure from 4-km samples centered about (a) the exterior inland breeze front and (b) the interior inland breeze front for the specific humidity, potential temperature, ozone, and wind components parallel ($\tilde{u}$) and perpendicular ($\tilde{v}$) to the flight path. The locations of the inland breeze fronts are indicated by the large arrows in Fig. 3.

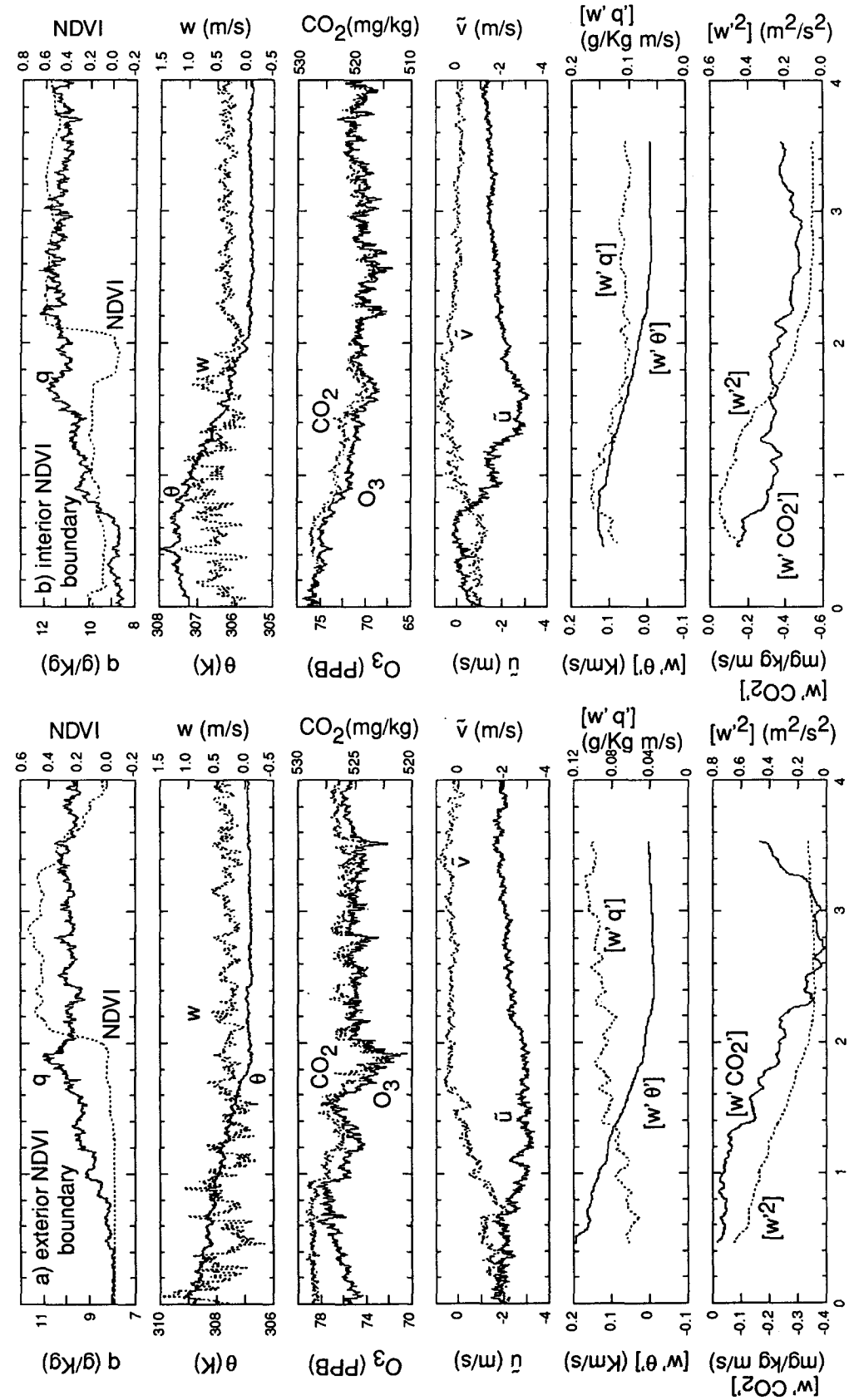

FIG. 6. Composited structure from 4-km samples centered about the NDVI boundaries (a) adjacent to the large bare field and (b) adjacent to the intensely irrigated area (see small arrows in Fig. 3) where u and v are the wind components parallel and perpendicular to the flight path, respectively.

could not be accurately estimated. The growing top of the internal boundary layer grows upward past the aircraft level within a few hundred meters downstream from the surface discontinuity. The downstream growth of the depth of the internal boundary layer due to a step change of surface heating is usually empirically modeled as a power-law dependence on downstream distance (Sutton 1934; Brutsaert 1982; Garratt 1990, p. 187; Antonia et al. 1977).

Following Brutsaert (1982) and others, the disturbance forced by the change of surface conditions is assumed to propagate vertically at a rate proportional to the magnitude of the vertical velocity fluctuations $\sigma_w(w^*, u^*)$ where $w^* = [(g/T_0)[w'T']h(x)]^{1/3}$ is the free-convection velocity scale, $h(x)$ is the top of the internal boundary layer, and u^* is the surface friction velocity. Then

$$dh(x)/dx = C\sigma_w(w^*, u^*)/U(x), \qquad (10)$$

where $U(x)$ is the total time-averaged flow perpendicular to the surface discontinuity and C is a nondimensional coefficient. Here $U(x)$ is sometimes assigned to be the flow at the top of the internal boundary layer (Jensen 1978). This slope can be roughly interpreted as that for a parcel rising at speed σ_w and advected at speed $U(x)$. That is, the growth of the internal boundary layer is interpreted as tilting of the thermally modified column as described in Anthes (1984).

If the spatial dependence of $\sigma_w(w^*, u^*)$ and $U(x)$ could be estimated, then (10) could be integrated to obtain the dependence of the depth of the internal boundary layer on downstream distance. Once the aircraft has intersected the internal boundary layer, the vertical velocity variance at the 33-m level increases roughly linearly with distance downstream (Fig. 6). Then using

$$\sigma_w(w^*, u^*) = \text{const}\, x^{1/2}$$

and assuming constant $U(x)$, (10) predicts

$$h(x) = \text{const}\, x^{3/2}. \qquad (10a)$$

Perhaps coincidentally, this is the same power law predicted in the free-convection limit, as is evident from references cited in Brutsaert (1982, pp. 165–166), and close to the 1.4 exponent found by Rao (1975) for the limit of free convection. The exponent is greater than unity because the growth rate increases in the downstream direction in response to increasing turbulence energy.

The coefficient C in (10) is now estimated from the average slope between the surface discontinuity and the intersection of the aircraft at 33 m with the internal boundary layer at distance Δx downstream from the surface discontinuity. This estimate yields an average slope of $\Delta x/33$ m. The intersection of the aircraft with the internal boundary layer is most easily detected in terms of temperature fluctuations although velocity fluctuations offer useful supplementary information. Since the position of this intersection varies between runs, the intersection in the composited time series is somewhat diffuse (Figs. 5–6). The variation of the location of intersection between aircraft runs is due partly to transient mesoscale variations of the horizontal wind on a timescale of 1–1.5 h (Mahrt et al. 1993) and presumably also due to time variation of the strength and location of the thermals just downstream from the surface discontinuity.

Based on composited temperature, the intersection of the aircraft with the top of the internal boundary layer occurs typically 150 m downstream from the surface discontinuity. This implies that the average slope is about 0.2. In the internal boundary layer over the heated surface, $\sigma_w(w^*, u^*)$ is about 0.5 m s^{-1} based on flow observed downstream from the intersection of the internal boundary layer with the aircraft. In this region $U(x)$ is about 2.25 m s^{-1} (Fig. 5). These values suggest that the value of C in (10) is about 0.9. These values correspond to a value of the constant in (10a) of about 0.02.

Similar calculations were made using repeated aircraft flights at approximately 30, 60, and 90 m over an interface between vineyards and dry ground without active vegetation (flight 17, 27 July 1991; MacPherson 1992). The slope of the internal boundary was computed from the three aircraft levels. The slope was estimated to be about 0.15, and $\sigma_w(w^*, u^*)/U(x)$ was estimated to be 0.17. This leads to a value of C in (10) of a little less than unity.

These slopes are an order of magnitude steeper than the usual 1/100 for growth of the internal boundary layer for neutral stratification (Brutsaert 1982). The steepness of the slope is due to the influence of heating and the weak wind speed and is consistent with the stability dependence predicted by Leclerc and Thurtell (1990) and others.

b. Spatial distribution of fluxes

Once the aircraft has intersected the internal boundary layer, the heat flux and vertical velocity variance, as measured at the 33-m level within the internal boundary layer, roughly increase linearly with distance downstream from the interior surface discontinuity (Fig. 6). The linear increase of the heat flux and vertical velocity variance downstream is apparently due to the buoyancy generation of turbulence energy.

The spatial variation of the moisture flux is more complicated. The moisture flux reaches a maximum in the inland breeze over the dry surface about 1000 m downstream from the interior vegetation boundary (Fig. 6) where it is actually about 30% greater than over the irrigated area. It is unlikely that this large moisture flux is due to the evaporation from the dry underlying surface. It is more likely due to mixing between the moist inland breeze and the drier air above

the internal boundary layer. In the northerly flow above the inland breeze, the specific humidity is expected to be smaller, more characteristic of the area-averaged boundary layer. This average includes extensive dry areas (Fig. 2). As a result, the downdrafts penetrating into the inland breeze are characterized by smaller specific humidity and northerly momentum, characteristic of the large-scale flow. In fact, the momentum flux (not shown) reaches a maximum near the downstream location of maximum moisture flux. The large positive moisture flux in this region would then be due to dry downdrafts and moist updrafts associated with mixing between the inland breeze and overlying boundary-layer flow.

The suspected weak surface evaporation at the dry surface and the observed large moisture flux at the aircraft level implies strong vertical divergence of the moisture flux as sketched in Fig. 7. From a Lagrangian point of view, the air in the inland breeze becomes less moist in the downstream direction due to the strong vertical divergence of the turbulent moisture flux analogous to the "entrainment drying boundary layer" studied in Mahrt (1991). This vertical flux divergence can be examined in terms of the conservation equation for specific humidity. The local increase of moisture with time, $\partial q/\partial t$, is computed to be about two orders of magnitude smaller than the advection term in this transition region. Therefore, the large horizontal advection of moisture from the irrigated area is approximately balanced by the strong vertical divergence of the turbulent moisture flux.

Vertically integrating this balance,

$$\int [u](\partial[q]/\partial x)dz = [w'q']_{\text{sfc}} - [w'q']_{33\text{ m}}, \quad (11)$$

where x is directed in the downstream direction approximately parallel to the flight track. Noting that the specific humidity decreases by 3.0 g kg^{-1} in the first 2 km downstream from the surface discontinuity and that the inland breeze flow is about 2.25 m s^{-1} in this region, the left-hand side of (11) is

$$(3.0\text{ g kg}^{-1})/(2\text{ km})\ (2.25\text{ m s}^{-1})\ (33\text{ m}) = 0.11\ (\text{g kg}^{-1})\ (\text{m s}^{-1}), \quad (12)$$

where the moisture advection at the aircraft level is assumed to be representative of the layer between the surface and the aircraft level. The large value predicted by (12) implies that the moisture flux increases significantly between the surface and the aircraft level. Noting that the moisture flux at the aircraft level is about 0.12 (g kg^{-1}) (m s^{-1}) in this region and substituting into (11), the surface moisture flux is estimated to be 0.01 (g kg^{-1}) (m s^{-1}). As additional evidence, the moisture flux at the aircraft level over the dry land ahead of the inland breeze is on the order of 0.01 (g kg^{-1}) (m s^{-1}). Since the moisture advection is small in this region, the moisture flux at the aircraft level is thought to be a good estimate of the surface moisture flux ahead of the inland breeze. These estimates indicate that the large moisture flux at the aircraft level in the transition region behind the front is due almost exclusively to vertical divergence of the moisture flux. For the most exterior vegetation boundary, the moisture advection is estimated to be 0.08 (g kg^{-1}) (m s^{-1}), again suggesting significant vertical divergence of the moisture flux.

The above calculation indicates that a major fraction of the moisture flux at the aircraft level is due to mixing between the moist inland breeze and the drier air above the internal boundary layer, as sketched in Fig. 7. Therefore, the moisture flux in the surface layer cannot be exclusively related to the surface conditions, and surface-layer similarity theory is expected to be invalid even as an approximation. Furthermore, the moisture flux measured from towers and aircraft platforms as low as a few tens of meters above the ground cannot be used to estimate the surface flux in cases of strong advection associated with surface heterogeneity. In the present case, these transition zones are about 1–2 km wide and occupy about 15% of the total record.

The influence of temperature advection on the vertical variation of the heat flux is estimated from the present data to be smaller than that for moisture, and the local warming $\partial\theta/\partial t$ cannot be neglected. The cold air advection acts to enhance the decrease of the heat flux with height. In fact, the heat flux may even decrease to a slightly negative value at the top of the inland breeze due to mixing with the warmer air aloft. This vertical convergence of the heat flux leads to observed warming of the inland breeze as it flows over the heated ground. Therefore, the heat flux estimated at the aircraft level would have to be corrected for advection before quantitatively relating growth of the internal boundary layer to the surface heat flux.

5. Footprint adjustment

The footprint formulation relates scalar fluxes at an arbitrary observational level to surface conditions in the upstream direction. It can be used to account for the advective phase shift of measured fluxes above the surface to improve the relationship between measured fluxes and surface conditions (Schuepp et al. 1992). This phase correction is analogous to the use of (11)–(12) to adjust the measured fluxes for advective effects. The weighted spatial integration inherent in the footprint calculation also removes some of the noise due to inadequate sampling of the measured fluxes.

With respect to a given surface source, the maximum influence observed at level z_m occurs downstream from the surface source at a distance of (Schuepp et al. 1992)

$$x_{\max} = \phi z_m/2 = Uz_m/(2ku^*), \quad (13)$$

where U is the average velocity between the surface

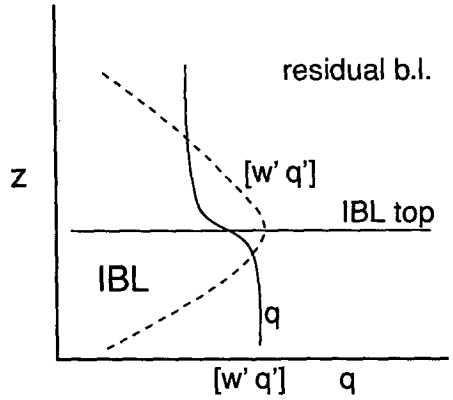

FIG. 7. Sketch of plausible vertical distribution of the moisture flux.

and the observational level. The slope of maximum influence of a given surface feature, dz^*/dx, can be estimated as x_{max}/z_m. From (13) this slope becomes

$$dz^*/dx = 2ku^*/U, \tag{14}$$

where z^* is the height of a sloping line (surface) of maximum influence associated with a given point (line) source at the surface. With footprint adjustment of the aircraft fluxes, each surface point within the domain is considered to be a source of heat or moisture.

Relationship (14) is the same mathematical form as the theoretical growth of the internal boundary layer due to a roughness change for the case of neutral stability. For this case, the growth rate of the internal boundary layer is expected to be proportional to u^*/U (e.g., Garratt 1992, p. 111). This growth rate describes the thickening of the internal boundary layer downstream from a surface discontinuity. The top of the internal boundary layer, h, represents the upper limit of the influence of the new surface, which must be higher than the surface of maximum influence z^*. Therefore, for a surface point just downstream from the surface discontinuity, $z^* < h$.

With daytime conditions, vertical diffusion is usually generated both by buoyancy generation and shear generation of turbulence. Therefore, instead of u^*, the standard deviation of the vertical velocity fluctuations σ_w is used as a velocity scale. Then (14) can be written in a more general form as

$$dz^*/dx = C^*\sigma_w/U, \tag{15}$$

where C^* is a nondimensional coefficient. This relationship is the same mathematical form as that for growth of the internal boundary layer in (10). The similarity of the growth of the internal boundary and the footprint approach is anticipated from the original derivation of the footprint formulation from diffusion of material emitted at the surface. The analogy between diffusion from a surface source and growth of the internal boundary layer was used in Elliot (1958) and Jackson (1976).

First, the value of C^* is estimated by approximating the slope of maximum influence as

$$dz^*/dx = 33 \text{ m}/\text{lag}_{max},$$

in which case C^* is estimated from (15) as

$$C^* = 33 \text{ m } U/(\sigma_w \text{ lag}_{max}), \tag{16}$$

where lag_{max} is the lag of maximum correlation between the flux at the aircraft level (33 m) and the NDVI. For flight 19, the flow is approximately parallel to the flight path but reverses sign in the center of the main irrigated region. Therefore, the flight path is divided into two parts of roughly constant wind direction and the lagged correlation function for the fluxes and NDVI are computed for each part. The lagged correlations for different fluxes are more similar to each other for the eastern part, chosen for the following calculations. The flux is again computed as the product of deviations from a running mean over a 375-m window. To compute the spatial dependence of the flux, the center of the window is incrementally translated between flux calculations. The flux is then correlated with different lags of the NDVI.

The lagged correlation between the heat flux and the NDVI shows a peak at a lag of about 100 m (Fig. 8a). A poorly defined peak occurs for the moisture flux at about 225 m (Fig. 8b). Choosing a value of lag_{max} = 150 m and using average values for the entire leg of $\sigma_w = 0.45 \text{ m s}^{-1}$ and $U = 1.4 \text{ m s}^{-1}$, C^* in (15) is estimated to be 0.65. The value of C^* is expected to be less than the value of C in (10), since the surface of maximum influence originating from a surface discontinuity should be below the top of the internal boundary layer (surface of highest detectable influence). Although C^* is estimated to be 0.65 and C is estimated to be 0.90, the statistical significance of this difference is not known. The comparison is complicated by uncertainties in the numerical evaluation of (10) and (15) and that the estimate of C^* uses statistics for the entire flight path while the estimation of C is based on the growth of the internal boundary layer in the transition regions.

The slowness of the decrease of the lagged correlation with increasing lag appears to be due to the slow decrease of the autocorrelation coefficients for the NDVI and surface heat flux (Fig. 8a). This slowness is due to the large scale of the heterogeneity (kilometers), which is significantly larger than the scale of the main turbulent eddies (hundreds of meters).

Alternatively, C^* might be estimated by footprint adjusting the NDVI. Footprint adjustment of the NDVI was used in Cihlar et al. (1992). Here, the NDVI is footprint adjusted by integrating (1) over discrete intervals of 3.5 m in which case

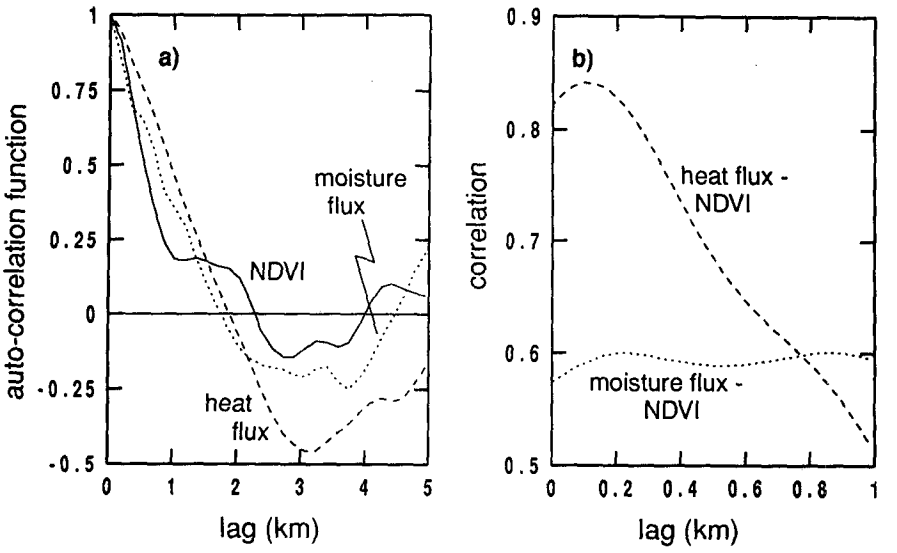

FIG. 8. (a) Lagged autocorrelation functions for the NDVI, heat flux, and moisture flux and (b) lagged correlations between the heat flux and NDVI and the moisture flux and the NDVI.

$$F(x_j, z_m) = \sum_{i=1}^{I} Q^*(x_i)\mathrm{IFP}(x_i, z_m), \qquad (17)$$

where $\mathrm{IFP}(x_i, z_m)$ is the footprint function integrated over the data interval defined by Eq. (5) of Schuepp et al. (1992), x_i are the set of points upstream from the flux observation at point x_j, $F(x_j, z_m)$ is footprint adjusted NDVI at point x_j at the aircraft level, and $Q^*(x_i)$ is the actual NDVI at the surface. The footprint-adjusted NDVI, $F(x_j, z_m)$, attempts to predict the integrated upstream NDVI, which influences the flux at x_j due to the communication between the aircraft level z_m and the surface through wind and turbulent diffusion.

To estimate the horizontal scale of the footprint adjustment $x_{\max}$ in (13), Eq. (17) is evaluated separately for different values of the scaling factor ϕ, as carried out in Schuepp et al. (1992). The scaling factor of maximum correlation ϕ^* is chosen by plotting the correlation between the flux and the footprint-adjusted NDVI (Fig. 9) as a function of the scaling factor ϕ. The spatial shift of maximum influence, $x_{\max}$, is then computed from the scaling factor of maximum correlation ϕ^* using (13). The scaling factor of maximum correlation for the heat flux (Fig. 9a) is between 2 and 3, corresponding to a value of $x_{\max}$ of about 40 m. The value of $x_{\max}$ for the moisture flux is about 300 m. However, the correlation between the flux and the footprint-adjusted NDVI varies slowly with scaling factor ϕ (note that the vertical coordinates in Fig. 9 are stretched). The correlation between the fluxes and the NDVI also varies slowly with changing scaling factor ϕ in Schuepp et al. (1992, their Fig. 4) where the fluxes were (inverse) footprint adjusted.

Since the lagged correlation between the moisture flux and NDVI does not show a well-defined maximum with respect to lag (Fig. 8b), translating the NDVI field in space should not improve the correlation. The improved correlation of the moisture flux with the NDVI due to the footprint adjustment of the NDVI apparently results from the integrating (smoothing) role of the footprint adjustment. In other terms, the footprint adjustment is a transform or mapping function that both translates and smooths the signal. In the present case of weak winds, the integrating role appears to be more important for the moisture flux–NDVI correlation.

For the heat flux–NDVI relationship, the translation part of the footprint adjustment may be significant since the lagged correlation between the NDVI and heat flux is maximum with a lag of about 100 m. However, the fact that the optimum scaling distance $x_{\max}$ (13) for the footprint function is only 40 m suggests that the integrating role may be the most important feature of the footprint adjustment for the heat flux as well. Similarly, Desjardins et al. (1992) concluded that for their data, the main influence of the footprint adjustment of the fluxes is to smooth the flux estimates. This multiple role of the footprint adjustment suggests that the physical meaning of $x_{\max}$ is ambiguous. Separation of the integrating (dispersion) role from the translation role of the footprint adjustment would require a two-parameter scheme. The dispersion effect is proportional to the strength of the turbulence, which for parts of the present flight track is presumably more related to the free-convection velocity scale than the mean wind speed. The translation part of the footprint adjustment is described by the mean wind speed. In the neutral case, the strength of the turbulence is proportional to the wind speed, so that the dispersion effect is proportional to the wind speed and the appropriate footprint adjustment can be described by one adjustable scaling factor

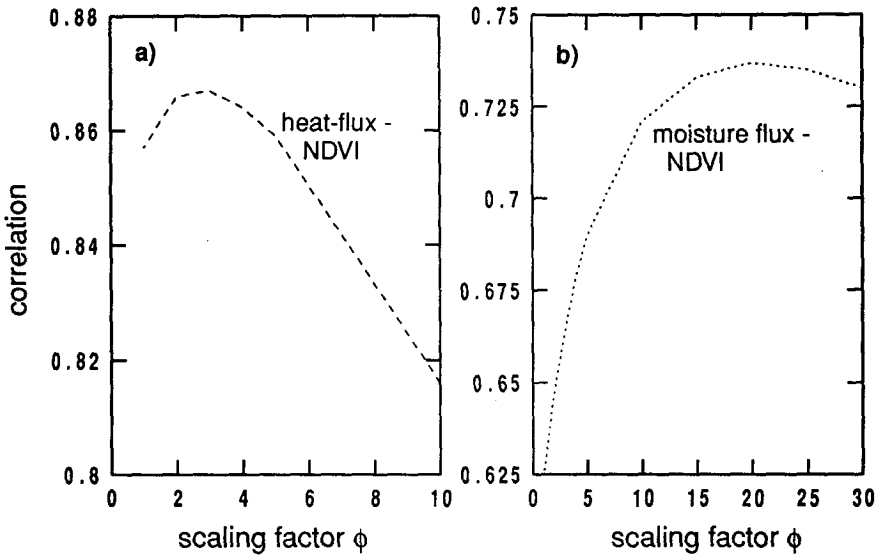

FIG. 9. Correlation between (a) the heat flux and the footprint-adjusted NDVI and (b) the moisture flux and adjusted NDVI, both as a function of the scaling factor ϕ.

ϕ. This is not the case however for the present data where surface heating is locally large and winds are weak.

6. Conclusions

With weak ambient flow (2 m s^{-1}), the irrigated area generates a cool moist inland breeze that flows outward from the center of the irrigated area. On the day with stronger ambient flow, about 4 m s^{-1}, the irrigated area does not generate a well-defined inland breeze but does induce significant diffluence of the ambient flow.

As the inland breeze flows out over the warmer, drier surrounding land, an internal boundary layer develops within the inland breeze. The internal boundary layer appears to grow to the top of the inland breeze, which then terminates at a well-defined inland breeze front located about 1 1/2 km downstream from the change of surface conditions. Fronts form outside both eastern and western boundaries of the irrigated area. An inland breeze also flows from a region of mixed surface conditions to a large region of warm bare soil and leads to a second breeze front over the warm soil. The breeze fronts are defined by sharp spatial change of horizontal momentum, moisture, carbon dioxide, and ozone and modest change of temperature. The fronts are maintained by both horizontal convergence and downward mixing of ambient momentum on the warm dry side of the front. The breeze fronts remained well defined throughout the observational period of 1045–1245 solar time.

The observations indicate that the vertical motion and attendant vertical transport are important only in the immediate vicinity of the front but contributes modestly to the horizontally averaged fluxes. The mesoscale flux at the 33 m flight level is about 15% of the turbulent flux. Although not as large as in some modeling studies, this flux must be included in order to compare aircraft fluxes with surface fluxes.

In the inland breeze downstream from the surface wetness discontinuity, strong horizontal advection of moisture is associated with a rapid increase of the turbulent moisture flux with height. This large moisture flux appears to be partly due to mixing between the thin moist inland breeze and drier air in the overlying residual boundary layer. As a consequence of the strong vertical divergence of the flux in the transition regions, the fluxes measured even as low as a few tens of meters are not representative of the surface fluxes. Consequently, use of the aircraft fluxes to estimate surface fluxes must be corrected in transition regions for advection between the aircraft level and the surface, and the estimate must include the mesoscale flux.

The spatial variability of the fluxes is interpreted within the footprint format. Attempts were made to compare predictions by footprint and internal boundary-layer approaches. Because of the weak winds, the scaling factor of maximum correlation for the footprint function appears to be mainly determined by the integrating (smoothing role) of the footprint adjustment rather than the translating role of the footprint adjustment.

Acknowledgments. The authors gratefully acknowledge Roni Avissar, Peter Schuepp, and an unknown reviewer for their valuable comments. This material is based upon work supported by Grant DAA H04-93-G-0019 from the Army Research Office and Grant ATM-8912736 from the Physical Meteorology Program of

the National Science Foundation. The field program was sponsored by the California Air Resources Board. Funding for the Twin Otter research aircraft was provided by the San Joaquin Valley Air Pollution Study Agency, in collaboration with the Pacific Gas and Electric Company, The Electric Power Research Institute, and the California Air Resources Board, and by the National Research Council of Canada.

REFERENCES

André, J. C., P. Bougeault, J.-F. Mafouf, P. Mascart, J. Noilhan, and J.-P. Pinty, 1989: Impact of forests on mesoscale meteorology. *Philos. Trans. Roy. Soc. London,* **B324,** 407–422.

Anthes, R. A., 1984: Enhancement of convective precipitation by mesoscale variations in vegetative covering in semi-arid regions. *J. Appl. Meteor.,* **23,** 541–554.

Antonia, R. A., H. Q. Danh, and A. Prabhu, 1977: Response of a turbulent boundary layer to a step change in surface heat flux. *J. Fluid Mech.,* **80,** 153–177.

Avissar, R., and F. Chen, 1993: Development and analysis of prognostic equations for mesoscale kinetic energy and mesoscale (subgrid-scale) fluxes for large-scale atmospheric models. *J. Atmos. Sci.,* **50,** 3751–3774.

Bechtold, P., J.-P. Pinty, and P. Mascart, 1991: A numerical investigation of the influence of large-scale winds on sea breeze and inland breeze type circulations. *J. Appl. Meteor.,* **30,** 1268–1279.

Betts, A. K., R. L. Desjardins, J. I. Macpherson, and R. D. Kelly, 1990: Boundary-layer heat and moisture budgets from FIFE. *Bound.-Layer Meteor.,* **50,** 109–138.

Bitan, A., 1981: Lake Kinneret (Sea of Galilee) and its exceptional wind system. *Bound.-Layer Meteor.,* **21,** 477–487.

Bougeault, P., B. Bret, P. Lacarrère, and J. Noilhan, 1991: An experiment with an advanced surface parameterization in a mesobeta-scale model. Part II: The 16 June 1986 simulation. *Mon. Wea. Rev.,* **119,** 2374–2392.

Brutsaert, W. H., 1982: *Evaporation into the Atmosphere.* D. Reidel, 299 pp.

Cihlar, J. P., H. Caramori, P. H. Schuepp, R. K. Desjardins, and J. I. MacPherson, 1992: Relationship between satellite-derived vegetation indices and aircraft-based CO_2 measurements. *J. Geophys. Res.,* **97,** 18 515–18 521.

Clark, T. L., T. Hauf, and J. P. Kuettner, 1986: Convectively forced internal gravity waves: Results from two-dimensional numerical experiments. *Quart. J. Roy. Meteor. Soc.,* **112,** 899–925.

Claussen, M., 1990: Area-averaging of surface fluxes in a neutrally stratified, horizontally inhomogeneous atmospheric boundary layer. *Atmos. Environ.,* **24a,** 1349–1360.

Dalu, G. A., and R. A. Pielke, 1993: Vertical heat fluxes generated by mesoscale atmospheric flow induced by thermal inhomogeneities in the PBL. *J. Atmos. Sci.,* **50,** 919–926.

——, ——, R. Avissar, G. Kallos, M. Baldi, and A. Guerrini, 1991: Linear impact of thermal inhomogeneities on mesoscale atmospheric flow with zero synoptic wind. *Ann. Geophys.,* **9,** 641–647.

Desjardins, R. L., P. H. Schuepp, J. I. MacPherson, and D. J. Buckley, 1992: Spatial and temporal variations of the fluxes of carbon dioxide and sensible and latent heat over the FIFE site. *J. Geophys. Res.,* **97,** 18 467–18 475.

Doran, J. C., and Colleagues, 1992: The Boardman Regional Flux Experiment. *Bull. Amer. Meteor. Soc.,* **73,** 1785–1795.

Elliot, W. P., 1958: The growth of the atmospheric internal boundary layer. *Trans. Amer. Geophys. Union,* **39,** 1048–1054.

Emanuel, K. A., 1983: On the dynamical definition(s) of "mesoscale." *Mesoscale Meteorology—Theories, Observations and Models.* D. K. Lilly and T. Gal-Chen, Eds., Reidel, 1–12.

Garratt, J. R., 1990: The internal boundary layer—A review. *Bound.-Layer Meteor.,* **50,** 171–203.

——, 1992: *The Atmospheric Boundary Layer.* Cambridge University Press, 316 pp.

——, and B. F. Ryan, 1989: The structure of the stably stratified internal boundary layer in offshore flow over the sea. *Bound.-Layer Meteor.,* **47,** 17–40.

Gash, J. H. C., 1986: A note on estimating the effect of limited fetch on micrometeorological evaporation measurements. *Bound.-Layer Meteor.,* **35,** 409–413.

Hadfield, M. G., W. R. Cotton, and R. A. Pielke, 1992: Large-eddy simulations of thermally forced circulations in the convective boundary layer. Part II: The effect of changes in wavelength and wind speed. *Bound.-Layer Meteor.,* **58,** 307–327.

Hechtel, L. M., C.-H. Moeng, and R. B. Stull, 1990: The effects of nonhomogeneous surface fluxes on the convective boundary layer: A case study using large-eddy simulation. *J. Atmos. Sci.,* **47,** 1721–1741.

Horst, T. W., and J. C. Weil, 1992: Footprint estimation for scalar flux measurements in the atmospheric surface layer. *Bound.-Layer Meteor.,* **52,** 279–296.

Hsu, H.-M., 1987: Study of linear steady atmospheric flow above a finite surface heating. *J. Atmos. Sci.,* **44,** 186–189.

Jackson, N. A., 1976: The propagation of modified flow downstream of a change in roughness. *Quart. J. Roy. Meteor. Soc.,* **102,** 924–933.

Jensen, N. O., 1978: Change of surface roughness and the planetary boundary layer. *Quart. J. Roy. Meteor. Soc.,* **104,** 351–356.

Leclerc, M. Y., and G. W. Thurtell, 1990: Footprint prediction of scalar fluxes using a Markovian analysis. *Bound.-Layer Meteor.,* **52,** 247–258.

Lilly, D. K., 1983: Mesoscale variability of the atmosphere. *Mesoscale Meteorology—Theories, Observations and Models.* D. K. Lilly and T. Gal-Chen, Eds., Reidel, 13–24.

MacPherson, J. I., 1992: NRC Twin Otter operations in the 1991 California Ozone Deposition Experiment. Rep. LTR-FR-118. Flight Research Laboratory, National Research Council, Ottawa, Canada, 41 pp.

——, R. W. H. Schmidt, A. M. Jochum, R. Pearson Jr., H. H. Neumann, and G. Den Hartog, 1993: Ozone flux measurement on the NRC Twin Otter during the 1991 California Ozone Deposition Experiment. *Proc. Eighth Symp. on Meteorological Observations.* Anaheim, CA, Amer. Meteor. Soc., 490–495.

Mahrt, L., 1991: Boundary-layer moisture regimes. *Quart. J. Roy. Meteor. Soc.,* **117,** 151–176.

——, and M. Ek, 1993: Spatial variability of turbulent fluxes and roughness lengths in HAPEX-MOBILHY. *Bound.-Layer Meteor.,* **65,** 381–400.

——, R. Desjardins, and J. I. Macpherson, 1993: Observations of fluxes over heterogeneous surfaces. *Bound.-Layer Meteor.,* **67,** 345–367.

Manqian, M., and J. Jinjun, 1993: A coupled model on land–atmosphere interactions—Simulating the characteristics of the PBL over a heterogeneous surface. *Bound.-Layer Meteor.,* **66,** 247–264.

Mason, P. J., 1988: The formation of areally-averaged roughness lengths. *Quart. J. Roy. Meteor. Soc.,* **114,** 399–420.

Noilhan, J., P. Lacarrère, and P. Bougeault, 1991: An experiment with an advanced surface parameterization in a mesobeta-scale model. Part III: Comparison with the HAPEX-MOBILHY dataset. *Mon. Wea. Rev.,* **119,** 2393–2413.

Oliveira, A. P., and D. R. Fitzjarrald, 1994: The Amazon River breeze and the local boundary layer: I. Observations. *Bound.-Layer Meteor.,* **63,** 141–162.

Pielke, R. A., 1984: *Mesoscale Meteorological Modeling.* Academic Press, 612 pp.

Pinty, J.-P., P. Mascart, E. Richard, and R. Rosset, 1989: An investigation of mesoscale flows induced by vegetation inhomogeneities using an evapotranspiration model calibrated against HAPEX-MOBILHY data. *J. Appl. Meteor.,* **28,** 976–992.

Rao, K. S., 1975: Effect of thermal stratification of the growth of the internal boundary layer. *Bound.-Layer Meteor.,* **8,** 227–234.

Raupach, M. R., 1993: The averaging of surface flux densities in heterogeneous landscapes. *Exchange Processes at the Land Surface for a Range of Space and Time Scales.* IAHS Publ. No. 212, H.-J. Bolle, R. A. Feddes, and J. D. Kalma, Eds., 343–356.

Raynor, G. S., S. Sethuraman, and R. M. Brown, 1979: Formation and characteristics of coastal internal boundary layers during onshore flows. *Bound.-Layer Meteor.,* **16,** 487–514.

Rotunno, R., 1983: On the linear theory of land and sea breeze. *J. Atmos. Sci.,* **40,** 1999–2009.

Schuepp, P. H., M. Y. Leclerc, J. I. MacPherson, and R. L. Desjardins, 1990: Footprint prediction of scalar fluxes from analytical solutions of the diffusion equation. *Bound.-Layer Meteor.,* **50,** 355–373.

——, J. I. MacPherson, and R. L. Desjardins, 1992: Adjustment of footprint correction for airborne flux mapping over the FIFE site. *J. Geophys. Res.,* **97,** 18 455–18 466.

Segal, M., and R. W. Arritt, 1992: Non-classical mesoscale circulations caused by surface sensible heat flux gradients. *Bull. Amer. Meteor. Soc.,* **73,** 1593–1604.

——, R. Avissar, M. C. McCumber, and R. A. Pielke, 1988: Evaluation of vegetation effects on the generation and modification of mesoscale circulations. *J. Atmos. Sci.,* **45,** 2268–2292.

——, W. E. Schreiber, G. Kallos, J. R. Garrat, A. Rodi, J. Weaver, and R. A. Pielke, 1989: The impact of crop areas in northeast Colorado on midsummer mesoscale thermal circulations. *Mon. Wea. Rev.,* **117,** 809–825.

Smith, B., and L. Mahrt, 1981: A study of boundary layer pressure adjustments. *J. Atmos. Sci.,* **38,** 334–346.

Sutton, O. G., 1934: Wind structure and evaporation in a turbulent atmosphere. *Proc. Roy. Soc. London, Ser. A,* **146,** 701–722.

Tsukamoto, O., J. Wang, and Y. Mitsuta, 1992: A significant evening peak of vapor pressure at an oasis in the semi-arid region. *J. Meteor. Soc. Japan,* **70,** 1155–1160.

Tucker, C. J., 1979: Red and photographic infrared linear combinations for monitoring vegetation. *Remote Sens. Environ.,* **8,** 127–150.

Wood, N., and P. J. Mason, 1991: The influence of stability on the effective roughness lengths for momentum and heat flux. *Quart. J. Roy. Meteor. Soc.,* **117,** 1025–1056.

Yan, H., and R. A. Anthes, 1988: The effect of variations in surface on mesoscale circulations. *Mon. Wea. Rev.,* **116,** 192–208.

Yoshino, M. M., 1975: *Climate in a Small Area.* University of Tokyo Press, 165–170.